Thompson, Adam and Körner, Lars and Senin, Nicola and Lawes, Simon and Maskery, Ian and Leach, Richard K. (2017) Measurement of internal surfaces of additively manufactured parts by X-ray computed tomography. In: 7th Conference on Industrial Computed Tomography (iCT 2017), 7-9 Feb 2017, Leuven, Belgium.

Measurement of internal surfaces of additively manufactured parts by X-ray computed tomography

Adam Thompson[1], Lars Körner[1], Nicola Senin[1,2], Simon Lawes[1], Ian Maskery[1], Richard Leach[1]

[1]Manufacturing Metrology Team, University of Nottingham, NG7 2RD, UK e-mail: ezxat1@nottingham.ac.uk

[2]Department of Engineering, University of Perugia, 06125, Italy

Abstract
Recent advances in X-ray computed tomography (XCT) have allowed for measurement resolutions approaching the point where XCT can be used for measuring surface topography. These advances make XCT appealing for measuring hard-to-reach or internal surfaces, such as those often present in additively manufactured parts. To demonstrate the feasibility and potential of XCT for topography measurement, topography datasets obtained using two XCT systems are compared to those from more conventional non-contact optical surface measurement instruments. A hollow Ti6Al4V part produced by direct metal laser sintering is used as a measurement artefact. The artefact comprises two component halves that can be separated to expose the internal surfaces. Measured surface datasets are compared by various qualitative and quantitative means, including the computation of ISO 25178-2 areal surface texture parameters. Preliminary results show that XCT can provide surface information comparable with more conventional surface measurement technologies, thus representing a viable alternative to more conventional measurement, particularly appealing for hard-to-reach and internal surfaces.

Keywords: additive manufacturing, surface topography, metrology

1 Introduction

Additive manufacturing (AM) is of growing interest to the manufacturing community, particularly for the ability of many AM technologies to produce parts containing complex geometries that were previously impossible to manufacture [1]. One significant barrier is the difficulty of applying core principles of quality assurance, such as dimensional and geometric inspection and verification, to additive parts [2]. In particular, in the inspection of AM surfaces, conventional optical and contact metrology solutions are often inadequate to measure hard-to-reach surfaces, and inapplicable for measuring internal surfaces. Such conditions are common with some of the most typical AM geometries, such as complex, hollow parts and lattice structures [3–5].

Over the past decade, X-ray computed tomography (XCT) has become a useful tool in holistic inspection of industrial parts. Efforts to incorporate XCT technology into the sphere of metrology have begun to make headway, especially in the acceptance and traceability of XCT machines as measurement instruments [6]. Although much work remains in standardising XCT for metrology (ISO 10360-11 [7] is still in the draft stages), XCT has begun to show promise for accurate measurement, particularly for verification of internal geometries present in AM parts [8]. Although the spatial resolutions typically achievable by XCT are not yet at the level generally required to capture the smaller-scale formations of a surface in addition to the overall shape, advanced systems are beginning to approach these resolutions in their best-case measurement scenarios. Because of these recent advances (such as improved detectors, more stable sources, smaller spot sizes), XCT is becoming an appealing option for measurement of surface topography. When considering AM parts featuring complex, internal geometries, the prospect of using XCT for surface topography measurement becomes even more appealing, as a method capable of overcoming the access requirement problems that are inherent with contact and optical measurement. The potential advantage of XCT is highlighted in a number of recent studies [9–13]. Specifically, Pyka *et al.* [9–11] performed the first investigations into the use of XCT for surface topography measurement, by extracting profiles from XCT slice data obtained from measurement of lattice struts. Townsend [12] and Thompson *et al.* [13] extended this work by initiating a more extensive examination of XCT topography measurement performance in comparison to conventional optical surface measurement. However, to date, no research effort has been specifically dedicated to investigate the challenges of measuring internal surfaces. In this paper, a preliminary investigation into XCT measurement of internal surfaces is presented.

2 Methodology

A hollow artefact fabricated via direct metal laser sintering (DMLS) is measured with two XCT systems as well as by additional non-contact optical measurement systems. The two industrial XCT systems available at the University of Nottingham are a Nikon Metrology MCT 225, and a Zeiss XRadia Versa XRM 500, each utilising scanning parameters optimised for each system. The artefact is fabricated via DMLS using an EOSINT M 280 in two separable parts (see figure 1). The artefact material is Ti6Al4V, chosen for industrial relevance and because it is known to be well suited to XCT measurement [8]. Once the two parts are assembled, the internal surfaces become inaccessible to conventional surface measurement solutions, and thus simulate the

metrological challenge of internal geometries that are present in many AM parts. When the two parts are separated, they can be inspected with more established texture measurement technologies, including coherence scanning interferometry (CSI, Zygo NewView 8300) and focus variation microscopy (FVM, Alicona InfiniteFocus G5). Surface topographies are extracted from XCT volumetric datasets by using the maximum gradient method [14] and compared with topography data obtained from the areal and profile topography measurement instruments. The comparison is based on first aligning the surface topographies obtained from each measurement, i.e. relocating them within the same measurement coordinate system. Topographies are then cropped to the same size, in order to ensure that the measurements refer to the same surface region. The shapes and sizes of topographic features of interest for the DMLS process (weld tracks, spatter, unmelted and partially melted particles) as they are reconstructed from each measurement, are compared using methods introduced in previous work [13]. Topographies are also subjected to an overall quantitative comparison via the computation of areal texture parameters (ISO 25178-2 [15,16]).

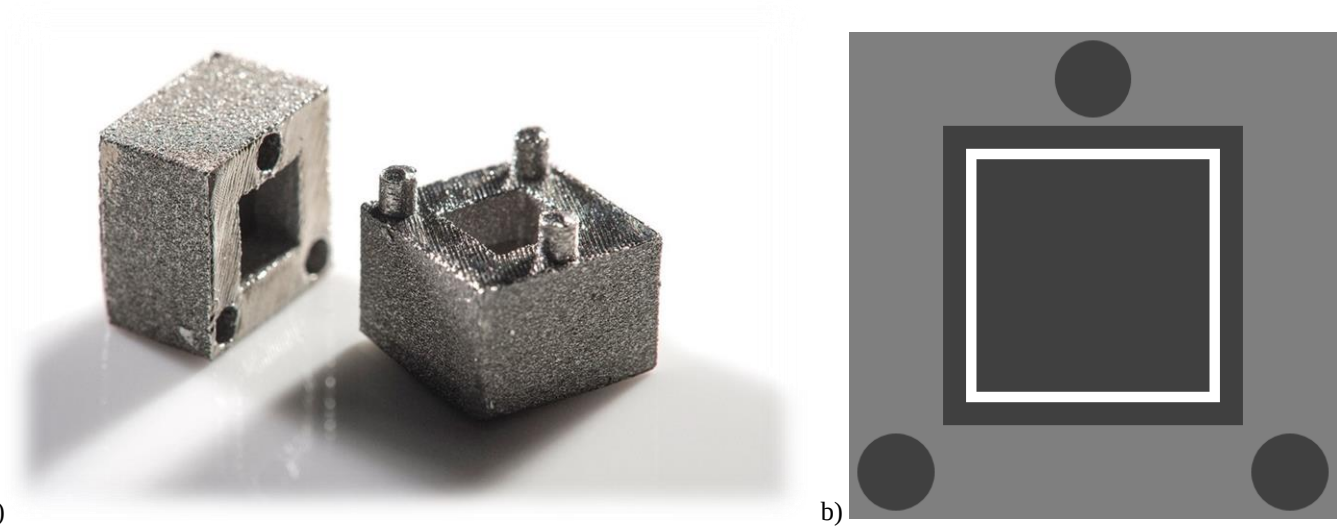

a) b)

Figure 1: a) Artefact for the measurement of internal surface texture. When assembled, cube dimensions are (10 × 10 × 10) mm, b) schematic diagram of the surface of interest (highlighted by the white square), as the recessed surface on the half of the cube containing three bores.

2.1 XCT measurements of surface topography

XCT measurements on the MCT system were performed using the following setup: voltage 150 kV, current 36 µA, exposure 2829 ms and geometric magnification 35×; yielding a voxel size of 5.7 µm after reconstruction. A warmup scan of approximately one hour was performed prior to the scan and a 0.25 mm copper pre-filter was used. X-ray imaging and volumetric reconstruction were performed using Nikon proprietary software (Inspect-X and CT-Pro, respectively), using filtered back projection with a second order beam hardening correction and a Hanning noise filter.

XCT measurements on the XRadia system were performed using the following setup: voltage 160 kV, current 63 µA and exposure 6000 ms. A geometric magnification of 5.75× and optical magnification of 0.4× were used, yielding a voxel size of 5 µm after reconstruction. A proprietary Zeiss HE3 pre-filter was also used. X-ray imaging and volumetric reconstruction were performed using Zeiss proprietary software (Scout-and-Scan and Reconstructor, respectively) using filtered back projection with no beam hardening correction and a smooth Gaussian reconstruction filter with a kernel size of 0.5. Reconstructed volumetric data were imported into VolumeGraphics VGStudioMAX 3.0 [17] and surfaces were determined using the maximum gradient method over four voxels; using the ISO-50 isosurface as a starting point [14].

2.2 Optical measurement of surface topography

Surface topography measurement systems and setups were chosen based on research performed previously by the authors in understanding a selective laser melted surface [13].

CSI measurements were performed using the CSI system and related proprietary measurement software (Zygo Mx). The 20× objective lens was used at 1× zoom (numerical aperture (NA) 0.40, field of view (FoV) 0.42 mm × 0.42 mm). Software data stitching was enabled to acquire a grid of ninety-five FoV, with 10 % lateral overlap. Vertical stitching was also applied, to merge two measurement *z* intervals (145 µm and 100 µm wide respectively with 10 µm overlap) in order to maximise vertical resolution over a large vertical range.

FVM measurements were performed and related proprietary measurement software was used (Alicona MeasureSuite). The 20× objective lens (NA 0.40, FoV 0.81 mm × 0.81 mm) was used with ring light illumination. Vertical resolution was set at 50 nm and lateral resolution at 3 µm. Software data stitching was enabled to acquire a grid of twelve FoV.

2.3 Topography data processing

XCT surface data were cropped to extract the surface of interest (see figure 1b) in VGStudioMAX, and outputted as triangulated meshes in .stl format. No simplification was performed in mesh generation. The triangulated meshes were rotated in MeshLab [18] to align the surface normal to the *z* axis (surface normal computed via principal component analysis [19] on the mesh point cloud), and exported again as an .stl. The rotated meshes were then imported into the surface metrology software MountainsMap by Digital Surf [20] and resampled into height maps, for comparison to topography datasets obtained from the optical measurement solutions. Resampling into height maps was performed in MountainsMap by projecting rays along the *z*-axis onto the triangulated mesh and recording the intersection points.

Height maps obtained by XCT and optical measurement were aligned (i.e. relocated in the same coordinate system) using MountainsMap. As the Zeiss XRadia system is not a metrology system, XRadia datasets were scaled in reference to CSI data (keeping proportions constant). All other datasets maintained their original sizes. For all the datasets, the following procedure was followed. From the aligned height maps, regions of size (1.5 × 1.5) mm were extracted, and levelled by least-squares mean plane subtraction. The extracted areas were filtered using a Gaussian convolution S-filter with 11 µm cut-off to remove small-scale surface features. The cut-off value was chosen as the minimum possible for the lowest lateral resolution height map (the MCT), representative of a grid of 4 × 4 pixels. A region size of (1.5 × 1.5) mm area was chosen as equal to the size of the region obtained from CSI measurement. At the used 20× magnification, the CSI region was obtained by stitching a large number of FoVs (ninety-five) and obtaining a larger area was deemed unfeasible due to the prohibitive number of stitching operations, excessive data sizes and measurement times. An F-operator was applied in the form of a Gaussian convolution filter, with 1.5 mm cut-off, to remove form error (waviness at larger scales) and obtain the SF surfaces (primary surfaces). Then, an L-filter (again based on Gaussian convolution) with 0.5 mm cut-off was applied to remove waviness; thus obtaining the SL surfaces (roughness surfaces). ISO 25178-2 areal texture parameters were calculated for both the SF and SL surfaces [15]. In addition, analyses on texture direction and power spectrum density were performed.

3 Results and discussion

3.1 Comparison of surface topography features

The comparison was performed on reconstructed top views of the SF height maps. For visual assessment, false colours (proportional to heights) were used in the reconstructions. Colour scales were homogenised by truncating height points above and below a common reference vertical range. Truncation was applied for visualisation purposes only, while the original datasets were maintained for quantitative comparison.

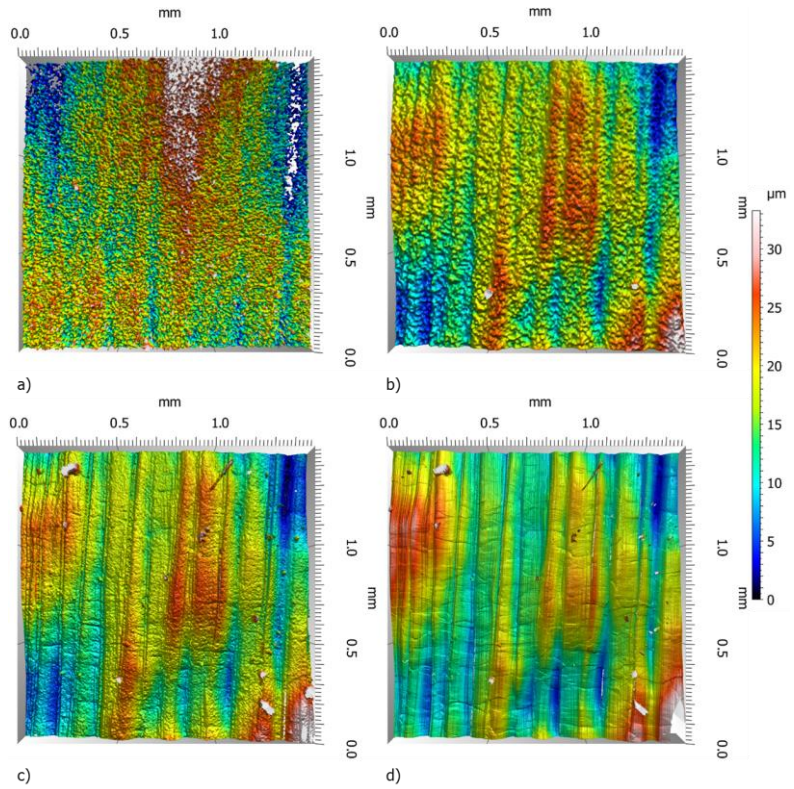

Figure 2: Levelled and truncated surface height maps: a) Zeiss XRadia XCT at 5.75× geometric and 0.4× optical magnification; b) Nikon XCT at 35× geometric magnification; c) FVM with 20× objective, ring light; d) CSI with 20× objective, 1.0× zoom

Visual investigation reveals similarities between the datasets. With the exception of the XRadia data, the topographies feature a similar rendition of the weld tracks and of larger-scale waviness components. The reconstruction of smaller-scale features, however, varies greatly between datasets. The FVM and CSI datasets are relatively equivalent, and the MCT system is capable of reconstructing some of the relevant topographic features (e.g. the weld tracks), although high-frequency noise is increasingly evident in the data when compared to optical measurement. The XRadia instrument returned the most noise, to the point where the main topographic features are barely visible.

3.2 Comparison of areal texture parameters

ISO 25178-2 [15] areal texture parameters were computed for the SF and SL surfaces. The results are presented in Tables 1 and 2 respectively. Only one region was analysed per surface type, leading to only one parameter value per measurement. The reported parameter values are, therefore, only indicative of the differences between the investigated datasets, and may not be statistically significant indicators of overall performance of a measurement solution compared to another. For the purpose of this comparison, parameters extracted from CSI data are used here as a reference measurement. Topography datasets were bandwidth-matched [21] (by cropping to the same sizes and using the same filtering operations with identical cut-offs); therefore, the differences should be ascribed to different behaviour of each measurement technology when interacting with the same measured surface region.

First, we examine parameters computed for SF surfaces, which should show trends consistent with what can be seen by visual observation of figure 2 (as the SF surface is the most similar to the visually reconstructed one). For the SF surfaces, the optical techniques return results that are the most similar to each other (*Sa* and *Sq* parameters differed by 1 % and 0.5 %, respectively). This is to be expected as both technologies are well established topographical measurement solutions. What is surprising is that the MCT system returns similar *Sa* and *Sq* parameters (within 1.5 % and 1.2 % respectively of the CSI parameters). Unfortunately, this result does not hold for the XRadia, where – despite the scale correction – the *Sa* and *Sq* parameters are more different (within 17 % and 20 % respectively of the CSI parameters). This is consistent with the results of visual observation of the reconstructed topographies (see figure 2) and indicates that the use of XCT for topography measurement should still be handled with care, as results may not necessarily be reliable. At this point it is not clear why the results from the XRadia system differ so substantially from the other systems used, and is likely due to a number of factors in the measurement.

The trend observed for *Sa* and *Sq* parameters generally holds for *Ssk*, *Sku*, *Sal* and *Std* parameters. The *Ssk* parameter of the SF surfaces varies between all instruments and was negative for the XRadia system and positive for the MCT and optical systems. The error of the XRadia system in this case has the additional side effect of providing further misleading information, because the change of sign implies a different balance of peaks and valleys in the topography (despite the effect not being particularly pronounced, as *Ssk* is basically zero in the XRadia data). The kurtosis of the topography height distribution (the *Sku* parameter) similarly differed noticeably between measurement instruments when compared to the CSI parameters (16 % for the XRadia, 24 % for the MCT and 10 % for the FVM parameters respectively). Data acquired by all instruments reported very similar values (within 0.1 % of the CSI parameter) for texture direction (the *Std* parameter). The autocorrelation length (the *Sal* parameter) for the XRadia data was within 3.8 % of the value calculated for CSI data as a percentage of the region width (1.5 mm), while *Sal* for the MCT system was within 0.5 %. The *Sal* value calculated for FVM data was within 0.1 % of the CSI parameter as a percentage of the region width (1.5 mm).

Parameter	Zeiss XRadia XCT	Nikon XCT	FVM	CSI
Sa	3.85 µm	3.25 µm	3.27 µm	3.30 µm
Sq	4.96 µm	4.09 µm	4.16 µm	4.14 µm
Ssk	-0.0472	0.1540	0.3680	0.5300
Sku	3.5	3.15	3.73	4.16
Std	85.7 °	85.7 °	85.8 °	85.8 °
Sal	0.168 mm	0.119 mm	0.110 mm	0.111 mm

Table 1: ISO 25178-2 [15] surface parameters for SF surfaces.

Following assessment of SF surfaces, we examine parameters computed for SL surfaces. For the SL surfaces, the optical techniques return results that are the most closely matched (*Sa* and *Sq* parameters differed by 3.6 % and 2.0%, respectively). The MCT in the SF case again system returns similar *Sa* and *Sq* parameters (within 1.6 % and 4.3 % respectively of the CSI parameters). This result again does not hold for the XRadia, where in this case the *Sa* and *Sq* parameters are within 36 % and 34 % respectively of the CSI parameters. The effect of the L filter in this case appears to be in exacerbating differences between calculated parameters, which may be due again to any number of an as-yet unclear reasons.

For SL surfaces, *Sa* and *Sq* parameters calculated for the XRadia data were 36 % and 34 % respectively larger than for the CSI data, while *Sa* and *Sq* parameters calculated for the MCT data were 1.6 % and 4.3 % respectively smaller than those calculated for the CSI data. The *Sa* and *Sq* parameters calculated for FVM data differed from CSI parameters by -3.6 % and -2.0% respectively. Similarly to the SF surface, the skewness of the SL surface varied greatly between instruments, though in this case

it was positive in all cases except for the MCT data. The *Sku* parameter showed greater variations between instruments than for SF surfaces, with deviations compared to the CSI parameter (-53 % for the XRadia, -46 % for the MCT and -11 % for the FVM parameters respectively). *Std* parameters exactly matched those calculated for SF surfaces. The *Sal* parameter for the XRadia system was within 1.1 % of the value calculated for the CSI as a percentage of the region width (1.5 mm), while *Sal* for the MCT system was within 0.5 %. The *Sal* value calculated from FVM data was within 0.2 % of the CSI parameter as a percentage of the region width (1.5 mm) in the SL case.

Parameter	Zeiss XRadia XCT	Nikon XCT	FVM	CSI
Sa	2.63 µm	1.90 µm	1.86 µm	1.93 µm
Sq	3.38 µm	2.42 µm	2.48 µm	2.53 µm
Ssk	0.1890	-0.0848	0.5440	0.4410
Sku	4.27	4.91	8.16	9.15
Std	85.7 °	85.7 °	85.8 °	85.8 °
Sal	0.0250 mm	0.0403 mm	0.0441 mm	0.0408 mm

Table 2: ISO 25178-2 [15] surface parameters for SL surfaces.

Although *Std* parameters are very consistent between datasets, surface texture direction analysis (see figure 3) reveals more information. Each plot represents the values of the angular power spectrum for the SL surfaces as a function of direction. The angle corresponding to the maximum value is taken as *Std*. These direction analyses show that, while the position of the primary peak (i.e. the *Std* parameter) is consistent between spectra, the ratio between the size of the primary peak and the smaller peaks (i.e. the signal to noise ratio) varies. This ratio is greatest in the CSI data and smallest in the XRadia data. As measurement noise is random and, therefore, devoid of direction, this can likely be attributed to greater noise in the XRadia measurement than in other datasets. It is clear that the values of the angular power spectrum are generally higher in multiple directions in the case of the noisier XRadia dataset, making it more difficult to isolate the highest peak. Despite the increased noise, however, isolation of this peak was still possible in the XRadia case. Noise in the Nikon data is much lower than in the XRadia data, but is visibly more substantial than in either of the optical measurements.

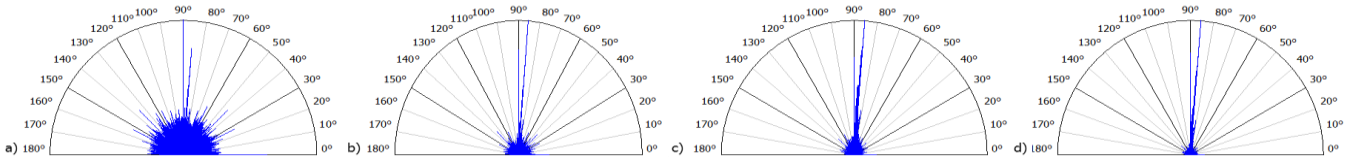

Figure 3: Surface texture direction of SL surfaces: a) Zeiss XRadia XCT; b) Nikon XCT; c) FVM; d) CSI

Further information about the SL surfaces can be provided by analysis of the averaged power spectrum densities (figure 4) of the surfaces. The plots are truncated at 2.5 µm height for ease of comparison. A number of elements are of interest in the averaged power spectrum density plots. FVM and CSI plots are very similar; both demonstrate an almost equivalent representation of the relevant topography frequencies as peaks can be observed corresponding to the main periodic features to be expected in a DMLS surface (e.g. weld tracks, represented by three peaks between 0.10 mm and 0.15 mm wavelengths). Some spectra carry more information at smaller scales (i.e. the size of the largest peak between 0.00 mm and 0.10 mm) than others. These peaks are typically a combination of smaller scale features and high-frequency noise. Interestingly, the position of the smallest-scale peak is shifted towards slightly larger wavelengths in the FVM dataset compared to the CSI dataset, which indicates a further attenuation of the smallest scales in FVM measurement. This is presumably due to the averaging mechanisms that implicitly take place in height determination via contrast, i.e. the way FVM operates (further investigation is in progress to better understand this observation). The MCT is again capable of capturing many of the same frequencies as the CSI and the FVM, albeit less strongly. The MCT averaged power spectrum density has a maximum slightly shifted towards the lowest frequencies, suggesting that the MCT system was not equivalently capable of capturing the highest frequency components of the topography when compared to CSI and FVM. Finally, consistent with all the previous observations, the XRadia system is the least capable of capturing the relevant frequencies of the topography.

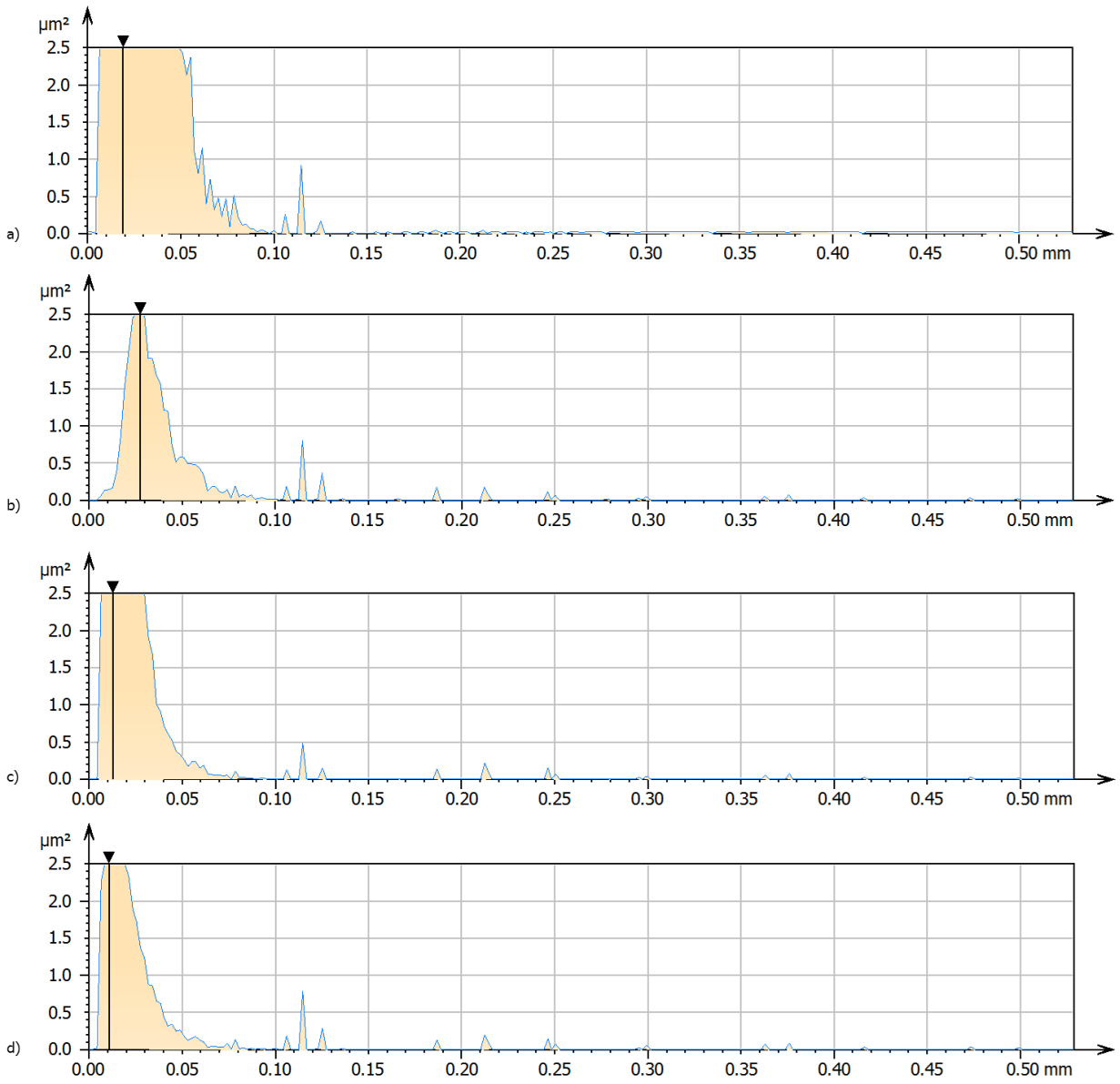

Figure 4: Averaged power spectrum densities of SL surfaces: a) Zeiss XRadia XCT; b) Nikon XCT; c) FVM; d) CSI

4 Conclusions and future work

Visual comparison showed notable similarities between all datasets, with the two optical systems showing the closest similarity (as could have been expected). However, MCT data were also visibly similar to those outputted by the two optical systems. XRadia data were not as similar; although some of the key features identifiable in other datasets could be identified in the XRadia data (i.e. weld track geometry).

Qualitative comparison of areal parameters calculated for SF and SL surfaces also showed similarity between values extracted from MCT and optical data. The MCT system demonstrates that topography measurement via XCT is viable. The XRadia system, however, demonstrates that XCT measurement of topography should be handled with care, as results may be unreliable, and expert assessment, appropriate utilisation, and skillful interpretation of results are still required. In terms of specific parameters, some are more robust than others (e.g. *Std*).

Our intention in performing this study was to qualitatively demonstrate the capability of XCT for surface topography measurement, particularly in reference to measurement of internal or otherwise difficult-to-access surfaces. As such, we have provided a preliminary assessment of this capability, through comparison of surface data extracted from two XCT systems with data extracted from conventional optical surface metrology instruments. It is clear that XCT may be a viable method of surface topography measurement, but performance may be strongly dependent on XCT instrument and set-up, as illustrated by the MCT and XRadia solutions. Regarding the quality of the XRadia data (in that the XRadia data were not particularly similar to the data acquired by other systems), it should be noted that these conclusions hold only for the particular measurement setup used. The

setup (as opposed to the instrument itself) may be the primary reason that the data were not particularly similar to those acquired using other systems, and further investigation is required to examine the cause of this problem. The XRadia data in this study serve to demonstrate the difficulty of acquiring reliable surface data from XCT.

The current limitations of this study should be noted. Primarily, as this study was based upon analyses of single measurements, significant work is yet to be performed in statistical testing of the methods used here in terms of measurement repeatability and reproducibility. As such, in their current state, no level of agreement or disagreement can be reported between results. Similarly, while the MCT system showed some qualitative agreement with the optical setups used, the XRadia system did not exhibit the same qualitative agreement and much work is yet to be performed in examining why this was the case. As such, a rigorous assessment of the minimum requirements of an XCT system used for surface topography applications is required. Variables examined in this assessment will include geometric magnification, sample material, image contrast and any of the myriad of other variables set during an XCT measurement.

Acknowledgements

AT, LK and RKL would like to thank the EPSRC (Grants EP/M008983/1 and EP/L01534X/1), 3TRPD Ltd. and Nikon Metrology for funding this work. NS and RKL would also like to thank the EC for supporting this work through the grant FP7-PEOPLE-MC METROSURF. The authors would like to thank Martin Corfield of the University of Nottingham, Faculty of Engineering for performing XRadia scans, and Digital Surf for providing the MountainsMap software.

References

[1] I. Gibson, D.W. Rosen and B. Stucker, Additive manufacturing technologies: 3D printing, rapid prototyping, and direct digital manufacturing (New York, NY, USA: Springer), 2014
[2] G. Ameta, R. Lipman, S. Moylan and P. Witherell, Investigating the role of geometric dimensioning and tolerancing in additive manufacturing J. Mech. Des., Vol 137, 111401, 2015
[3] R.K. Leach, Metrology for Additive Manufacturing, Meas. + Control, Vol 49, 132–5, 2016
[4] P.I. Stavroulakis and R.K. Leach, Review of post-process optical form metrology for industrial-grade metal additive manufactured parts, Rev. Sci. Instrum., Vol 87, 041101, 2016
[5] A. Townsend, N. Senin, L. Blunt, R.K. Leach and J.S. Taylor , Surface texture metrology for metal additive manufacturing: a review, Precis. Eng., Vol 46, 34–47, 2016
[6] L. De Chiffre, S. Carmignato, J.-P. Kruth, R. Schmitt and A. Weckenmann, Industrial applications of computed tomography, CIRP Ann. - Manuf. Technol., Vol 63, 655–77, 2014
[7] ISO 10360-11 DRAFT, Geometrical Product Specifications (GPS) - Acceptance and reverification tests for coordinate measuring machines (CMM) - Part 11: Computed tomography (International Organization for Standardization)
[8] A. Thompson, I. Maskery and R.K. Leach, X-ray computed tomography for additive manufacturing: a review, Meas. Sci. Technol., Vol 27, 072001, 2016
[9] G. Pyka, G. Kerckhofs, A. Braem, T. Mattheys, J. Schrooten and M. Wevers, Novel micro-CT based characterization tool for surface roughness measurements of porous structures, SkyScan User Meeting (Mechelen, Belgium: SkyScan User Meeting), 1–5, 2010
[10] G. Kerckhofs, G. Pyka, M. Moesen, S. Van Bael, J. Schrooten and M. Wevers, High-resolution microfocus x-ray computed tomography for 3D surface roughness measurements of additive manufactured porous materials, Adv. Eng. Mater., Vol 15, 153–8, 2013
[11] G. Pyka, A. Burakowski, G. Kerckhofs, M. Moesen, S. Van Bael, J. Schrooten and M. Wevers, Surface modification of Ti6Al4V open porous structures produced by additive manufacturing, Adv. Eng. Mater., Vol 14, 363–70, 2012
[12] A. Townsend, L. Blunt and P.J. Bills, Investigating the capability of microfocus x-ray computed tomography for areal surface analysis of additively manufactured parts, ASPE/euspen Conference: Dimensional Accuracy and Surface Finish in Additive Manufacturing (Raleigh, NC, USA), 2016
[13] A. Thompson, N. Senin and R.K. Leach, Towards an additive surface atlas, ASPE/euspen Conference: Dimensional Accuracy and Surface Finish in Additive Manufacturing (Raleigh, NC, USA), 2016
[14] J.J. Lifton, A.A. Malcolm and J.W. McBride, A simulation-based study on the influence of beam hardening in x-ray computed tomography for dimensional metrology, J. Xray. Sci. Technol., Vol 23, 65–82, 2015
[15] ISO 25178-2, Geometrical product specifications (GPS) -- Surface texture: Areal -- Part 2: Terms, definitions and surface texture parameters, 2012 (International Organization for Standardization)
[16] R.K. Leach, Characterisation of areal surface texture (Springer-Verlag), 2013
[17] Volume Graphics, VGStudio MAX, 2016, http://www.volumegraphics.com/en/products/vgstudio-max/ (accessed 14th December 2016)
[18] Visual Computing Lab - ISTI – CNR, MeshLab, 2016, http://meshlab.sourceforge.net/ (accessed 14th December 2016)
[19] I. Jolliffe, Principal Component Analysis, in Wiley StatsRef: Statistics Reference Online (Wiley), 2014
[20] Digital Surf, Mountains® surface imaging & metrology software, 2016, http://www.digitalsurf.com/en/mntkey.html (accessed 14th December 2016)

[21] R.K. Leach and H. Haitjema, Bandwidth characteristics and comparisons of surface texture measuring instruments, Meas. Sci. Technol., Vol 21, 32001, 2010